Desalination and Water Treatment
www.deswater.com

doi: 10.5004/dwt.2018.23090

129 (2018) 279–288
October

Carbonization of rubber (*Hevea brasiliensis*) seed shell by one-step liquid phase activation with H_2SO_4 for methylene blue adsorption

Ali H. Jawad

Faculty of Applied Sciences, Universiti Teknologi MARA, 40450 Shah Alam, Selangor, MALAYSIA, Tel. +60 3 55211721; emails: ahjm72@gmail.com, ali288@salam.uitm.edu.my

Received 31 August 2017; Accepted 8 September 2018

ABSTRACT

The rubber (*Hevea brasiliensis*) seed shell, which is an agricultural waste, was carbonized by one-step liquid phase activation with H_2SO_4 to be a potential bio-char adsorbent for methylene blue (MB) adsorption from aqueous solution. Carbonized rubber seed shell (CRSS) was characterized by a CHNS-O, Brunauer–Emmett–Teller (BET), X-ray diffraction, Fourier transform infrared spectroscopy, scanning electron microscope with an energy dispersive X-ray spectrometer (SEM–EDX), point-of-zero charge (pH_{pzc}), and proximate analyses. Batch mode adsorption studies were conducted by varying operational parameters such as adsorbent dosage (0.02–0.30 g), solution pH (3–11), initial MB concentrations (50–300 mg/L) and contact time (0–1,440 min). The equilibrium data were well correlated by Langmuir isotherm compared with Freundlich and Temkin models. The maximum adsorption capacity, q_{max}, of CRSS for MB adsorption was 208.3 mg/g at optimum pH 8 and temperature 303 K. The kinetic uptake profiles are well described by the pseudo-second-order model. All results mentioned above revealed that the CRSS can be feasibly utilized for the removal of MB from aqueous solution.

Keywords: Rubber seed shell; Carbonization; Chemical activation; Sulphuric acid; Adsorption; Methylene blue

1. Introduction

Wastewater from textile, rubber, paper, plastics, leather, and food industries contains dyes used to color their final products. The discharge of dye-contained wastewaters into ecosystem is a dramatic source of aesthetic pollution, eutrophication and perturbation in aquatic life as most of dyes are highly visible, stable and unaffected by chemical, photochemical as well as biological degradation [1–3]. By definition, basic dyes are cationic species originating from positively charged nitrogen or sulphur atoms. In fact, basic dyes are named because of their affinity to basic textile materials with net negative charge [4]. Methylene blue (MB) is a basic dye with favorable water solubility and the most commonly used dye in textiles and leather, printing calico, printing cotton, and biological staining methods [5]. Tinctorial value of MB is very high; even at concentration less than 1 mg/L a noticeable coloration is detected and can be classified as toxic colorants [6]. MB has various harmful effects on human beings, such as eye irritation, gastrointestinal irritation and nausea upon ingestion, including vomiting and diarrhea [7], so it is of utmost importance to be removed from wastewaters.

Various conventional technologies have been tested for the removal of dyes from industrial effluents and wastewaters, including bioremediation [8], electrochemical degradation [9], cation exchange membranes [10], Fenton chemical oxidation [11], and photocatalysis [12,13]. Most of these methods, nevertheless, pose techno-economical limitations for field-scale applications [14]. Comparatively, adsorption has been proved to be a well-established and most widely used technique among other water purification processes. Adsorption-based treatment with appropriate adsorbent materials shows high performance and selectivity, flexibility and simplicity of design, convenience of operation without producing harmful by-products as well as economically cost-effective [15].

Activated carbons (ACs) are materials containing large surface area, well-developed porosity and various functional groups. Therefore, AC has been widely utilized in versatile applications such as gas separation, solvents recovery, gas storage, super capacitors electrodes, catalyst support, adsorbent for organic and inorganic pollutants from drinking water, and so on [16]. However, a high cost of AC production limits its application in various technologies. Recognizing this economic obstacle, many investigators have made extensive efforts in low-cost alternatives to AC from a range of carbonaceous precursors, such as lignocellulosic materials [17], biopolymer [18], coal [19], char [20], and fruit peels [21]. The textural properties and adsorption capacities of carbonaceous materials are mainly depend on the nature of the starting martial, activation method, type of activator, and preparation conditions [22].

Chemical surface modification methods are widely used to prepare hydrophilic carbonaceous materials and biochar. Hydrophilicity of the carbonaceous materials is associated essentially with the presence of oxygen-containing groups on the surface such as carboxylic, phenolic, and lactonic groups. Sulphuric acid is a reagent frequently used to enhance oxygen content on the surface [23]. Researches demonstrated that the amount of oxygen-containing surface functional groups, specific surface area and pore structure highly depend on the concentration of activation agents. While oxygen content of carbonaceous materials usually increases with the increase of reagent concentration, the surface area and pore volume values decrease adversely [24]. Nowadays, interests are growing in the utilization of agricultural waste and food residues as low-cost and steady sources for developing rich carbonaceous materials with multifunctional functional groups that can be potentially used for removal of water pollutants.

Rubber (*Hevea brasiliensis*) seed shell (RSS) is an agricultural by-product of the rubber tree. The *Hevea* tree gives significant quantities of milk-like sap called latex, which is an emulsion of hydrocarbons in water. It is a material of industrial significance. Rubber seed oil is extracted from the rubber seed. Rubber seed oil is extracted from the rubber seed. The RSS is used as biofuel or manure or is discarded and allowed to rot. The economic importance of the rubber tree has largely focused on the rubber latex with little attention paid to the potential usefulness of its by-product [25]. While significant progress has been made in the development and utilization of modified agricultural by-product in water and wastewater treatment, there is little information on the potential for the application of these by-products [26]. RSS, a waste agricultural by-product, is utilized in Malaysia as fuel and manure [27].

Therefore, the key objective of this study is to develop a renewable low-cost adsorbent from carbonized rubber seed shell (CRSS) by one-step liquid phase activation with H_2SO_4 at relatively low temperature (~105°C). Another purpose of this work is to evaluate the effectiveness of the CRSS for removing large molecules of cationic dye such Methylene blue (MB). Due to carbonization process with H_2SO_4, the CRSS surface would be SO_3H group–rich and may be favorable for the adsorption of MB through electrostatic interaction. Sulphuric acid (H_2SO_4) is frequently used as a low-cost chemical agent for the preparation of carbonaceous adsorbents from ligno-cellulosic materials such as coconut leaves [17], mango peel [21], *Euphorbia rigida* [28], bagasse [29], almond husk [30], parthenium hysterophorus [31], sunflower oil cake [32], pine-fruit shell [33], *Delonix regia* pods [34], wild carrot [35], *Ficus carica* [36], potato peel, and neem bark [37].

2. Materials and methods

2.1. Adsorbate

The cationic dye, methylene blue (MB) was used as an adsorbate in this work. MB was purchased from R&M Chemicals, Malaysia, with chemical formula ($C_{16}H_{18}ClN_3S.xH_2O$) and molecular weight (319.86 g/mol). Ultra-pure water was used to prepare all solutions.

2.2. Carbonization and characterization processes

RSS was collected from a rubber plantation estate in Pauh, Perlis, Malaysia, and was used as the precursor for the preparation of biochar in this work. The RSS was first washed with water to remove dirt and subsequently dried at 105°C for 24 h to remove the moisture contents. The dried RSS was ground and sieved to the size of 250–500 μm before mixing with concentrated H_2SO_4 (95%–98%). The mixing ratio was fixed at 1 g of dried RSS powder with 1 mL of concentrated H_2SO_4 and left inside an oven at 105°C for 24 h following the method reported by Garg et al. [38]. The CRSS was washed with hot distilled water until the filtrate water was clear reached a neutral pH value. The elemental analysis was carried out using a CHNS-O analyzer (Flash 2000, Organic Elemental Analyzer, Thermo Scientific, Netherlands). The oxygen contents were calculated by difference. X-ray diffraction (XRD) analysis was performed by XRD in reflection mode (Cu Kα radiation) on an X'Pert Pro X-ray diffractometer, PANalytical (UK). Scans were recorded with a scanning rate of 0.59°/s. The diffraction angle (2θ) was varied from 10° to 90°. Textural characterization of CRSS was carried out by N_2 adsorption using ASAP 2060, Micromeritics, USA. FTIR spectral analysis of CRSS was performed on a PerkinElmer (USA), Spectrum One in the 4,000 cm^{-1}–500 cm^{-1} wavenumber range. The surface physical morphology was examined by using scanning electron microscopy (SEM-EDX, TM3030Plus, Tabletop Microscope, Hitachi, Japan). The pH at the point-of-zero charge (pH_{pzc}) was estimated using a pH meter (Model 827 pH Lab, Metrohm, Switzerland), as described elsewhere [39].

2.3. Batch adsorption experiments

The batch adsorption experiments of MB adsorption onto CRSS surface were performed in a set of 250 mL Erlenmeyer flasks containing 100 mL of MB solution. The flasks were capped and agitated in an isothermal water bath shaker (waterbath model WNB7-45, Memmert, Germany) at fixed shaking speed of 110 stroke/min and 303 K until equilibrium was achieved. Batch adsorption experiments were carried out by varying several experimental variables such as adsorbent dosage (0.02 to 0.3 g), pH (3 to 11), initial dye concentration (50 to 300 mg/L) and contact time (0 to 1,440 min) to determine the best uptake conditions for adsorption. The pH of MB solution was adjusted by adding either 0.10 mol/L HCl or

NaOH. After mixing of the CRSS-MB system, the supernatant was collected with a 0.20 μm Nylon syringe filter and the concentrations of MB were monitored at a different time interval using a DR 2800 Direct Reading Spectrophotometer (HACH) at the maximum wavelength (λ_{max}) of absorption at 661 nm. As for the thermodynamic studies, the same procedures were repeated and applied at 313 K, 323 K, and 333 K with the other parameters set constant. The adsorption capacity at equilibrium, q_e, (mg/g) and the percentage of color removal, CR (%) of MB were calculated using Eqs. (1) and (2) as follows:

$$q_e = \frac{(C_o - C_e)V}{W} \quad (1)$$

$$CR\% = \frac{(C_o - C_e)}{C_o} \times 100 \quad (2)$$

where C_o and C_e (mg/L) are the initial and equilibrium concentrations of MB, respectively, V (L) is the volume of the solution, and W (g) is the mass of dry adsorbent used.

3. Results and discussion

3.1. Characterization of CRSS

3.1.1. Physical properties

The results of physical characterization of CRSS are recorded in Table 1. The ultimate results indicate that CRSS has a relatively high carbon and oxygen content with low surface area. The low surface area and porosity of CRSS can be attributed to the harsh liquid-phase oxidation conditions with concentrated H_2SO_4 (95%–98%) which is responsible for destructing pore walls of CRSS. In this respect, Jiang et al. [40] also found the similar result by preparing active carbon by using H_2SO_4 as a chemical activator at relatively a low temperature.

Table 1
Characterization of CRSS

Analysis	Values
Proximate analysis	
Bulk density g/mL	0.716
Ash content (wt %)	19.95
Moisture content (wt %)	6.21
Fixed carbon (%)	73.84
Elemental analysis (wt %)	
Carbon, C	55.75
Hydrogen, H	4.19
Nitrogen, N	1.51
Sulphur, S	Not detected
Oxygen, O (by difference)	38.55
Surface area	
Total pore volume($p/p^\circ = 0.990$) (cm^3/g)	0.0034
Mean pore diameter (nm)	13.91
BET surface area (m^2/g)	0.979

3.1.2. XRD analysis of CRSS

The XRD pattern of the CRSS is shown in Fig. 1. XRD pattern is indexed based on a standard diffraction reference pattern (PCPDF No: 898487). Appearance of a broad diffraction background and the absence of a sharp peak reveal a predominantly amorphous structure. Overall, there were two XRD peaks at 2θ = 24° (002) and 2θ = 42° (101) in the spectrum. These signatures relate to crystalline carbon with expanded lattice parameters (carbon with impurities).

3.1.3. FTIR spectral analysis

The pattern of MB adsorption onto CRSS is related to the availability of active functional groups and bonds of the CRSS surface. Thus, FTIR spectrum of CRSS before adsorption (Fig. 2(a)) shows various functional groups, in accordance with their respective wavenumber (cm^{-1}) position as reported in literature. The weak band observed around 3,500 cm^{-1} is assigned to the overlapping of the stretching

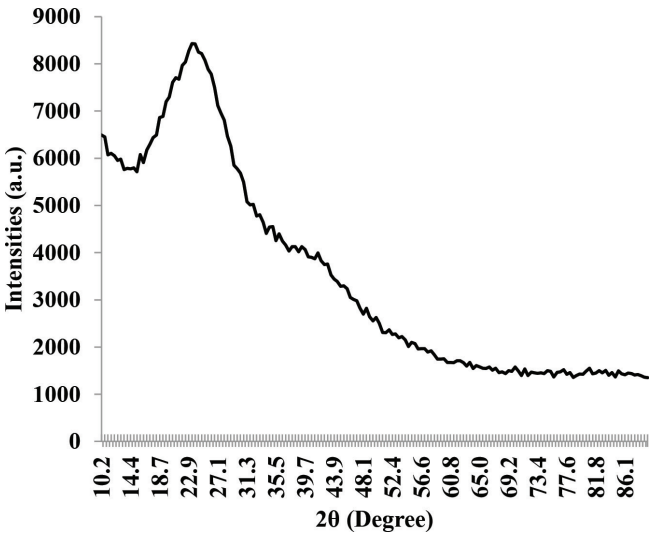

Fig. 1. XRD pattern of CRSS.

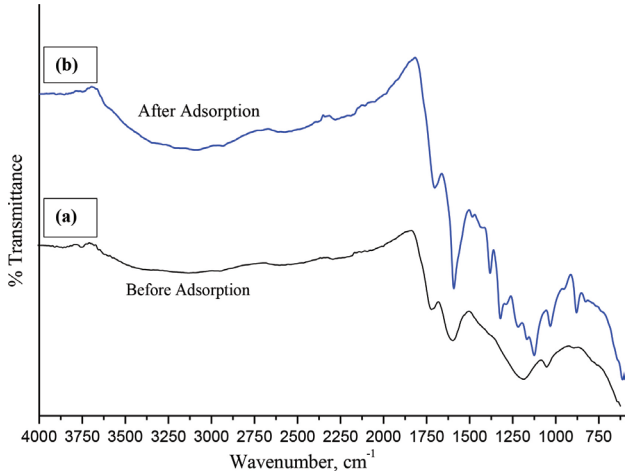

Fig. 2. FTIR spectra of CRSS: (a) before MB adsorption and (b) after MB adsorption.

vibration of N–H and O–H functional groups [41]. The band at about 1,700 cm^{-1} relates to C=O stretching of ketones, aldehydes, lactones or carboxyl groups, and the band at 1,600 cm^{-1}–1,580 cm^{-1} is assigned to C=C vibrations in aromatic rings [7]. The IR bands between 1,300 and 1,000 cm^{-1} are observed for oxidized carbon materials and are assigned to C–O and/or C–O–C stretching in acids, alcohols, phenols, ethers and/or esters groups and sulphonic acid groups (–SO_3) [17]. Thus, the FTIR spectrum of CRSS before adsorption indicates that the external surface of CRSS is SO_3H group–rich in addition to various functional groups, containing oxygen of carboxylic and carbonyl species. These active groups on CRSS surface are responsible for enhancing the adsorption of cationic species such as MB due to the electrostatic interaction. After MB adsorption, IR bands appear and many functional groups are undergone red or blue shifting (Fig. 2(b)). As can be seen, some of the bands shifted and became more pronounced in which the attenuated bands at about 1,650 cm^{-1} (–N–H bending), 1,380 cm^{-1} (C–N bending vibration), 850 cm^{-1} (–CH_2 vibration) suggest the interaction of MB molecules with the functional groups of CRSS.

3.1.4. SEM-EDX analysis

The SEM and EDX results of CRSS before and after adsorption are shown in Figs. 3(a) and (b), respectively. As can be seen in Fig. 3(a), the surface of CRSS appears to be highly porous and heterogeneous. Pores with different size and shape are also clearly visible. The pores are generated due to H_2SO_4 activator, which was responsible for the porosity development of the raw RSS by creating new pores. Therefore, the resulting pore structure is suitable for

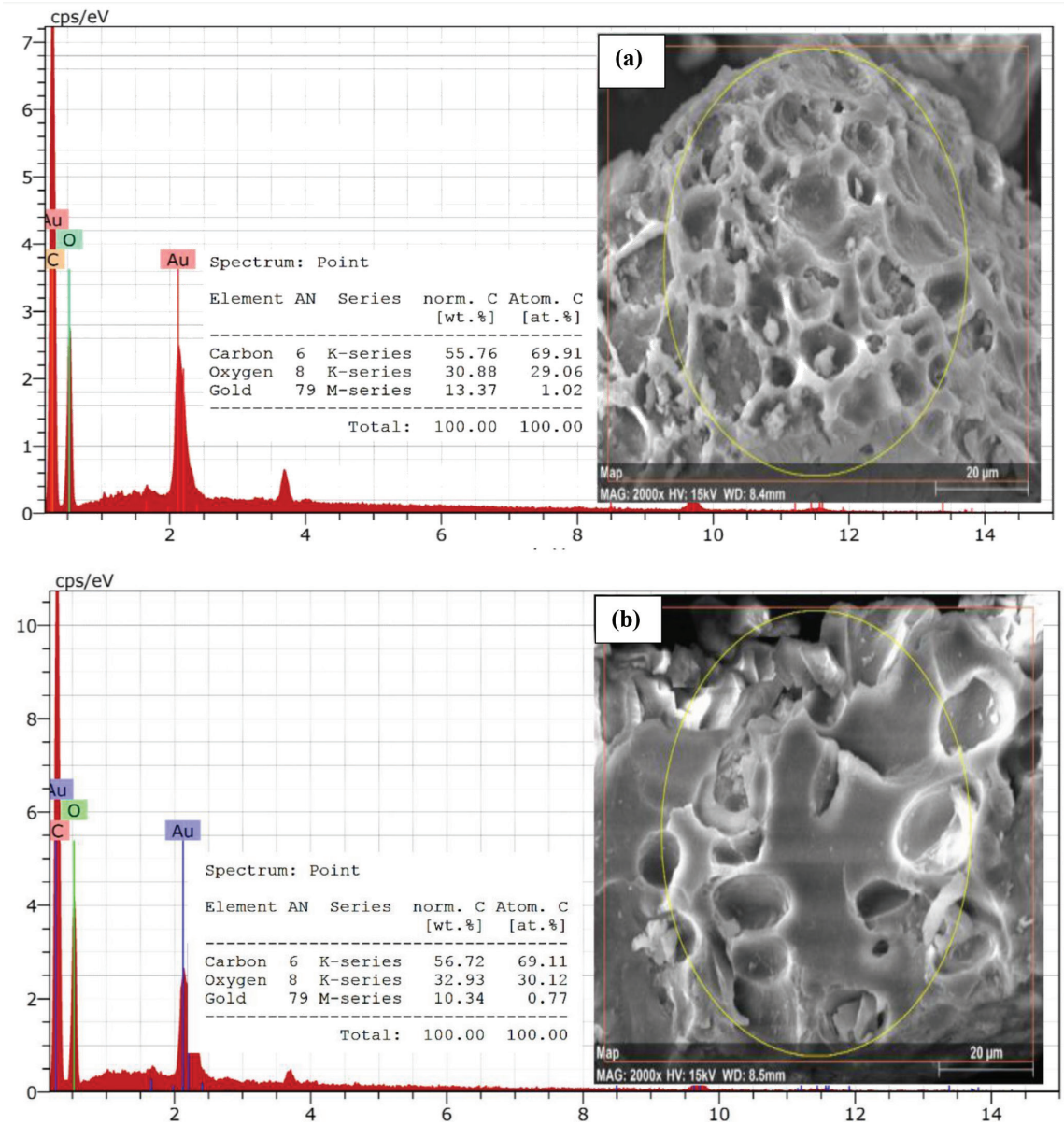

Fig. 3. Typical SEM micrograph of CRSS at 3.0K magnifications: (a) before MB adsorption, and (b) after MB adsorption.

the adsorption of MB within the pore structure of CRSS. Additionally, the corresponding EDX spectrum indicates that the CRSS surface consists of mainly C and O. After MB adsorption, the CRSS surface is altered to be more compact and less open pores are seen due to loading of MB molecules on the CRSS surface. Noteworthy, the presence of Au peaks in all spectra is due to the gold purposely settled to increase electric conduction and to improve the quality of the images.

3.1.5. Point-of-zero charge

Fig. 4 shows the pH_{pzc} results of the experiments performed with the CRSS, where the pH ranged from 2 to 12. The pH_{pzc} of the CRSS was 4.2, which indicates the acid character of the CRSS surface, in agreement with the presence of acid groups from the FTIR results (Fig. 2(a)). In general, the adsorption of anions is favored at solution pH below the pH_{pzc} value as the surface of CRSS is positively charged due to protonation whereas at solution pH above the pH_{pzc} value, the surface of CRSS becomes negatively charged and thus, adsorption of cations is preferred. In this respect, Jawad et al. reported that the pH_{pzc} values of the coconut leaf and mango peel treated with H_2SO_4 were 3.20 [17] and 4.60 [21], respectively. Furthermore, Karagöz et al. [32] reported that the pH_{pzc} value lies between pH 2.5 and 5.5 which was attributed to the acid form of AC derived from sunflower oil cake treated with H_2SO_4.

3.2. MB adsorption

3.2.1. Effect of the adsorbent dosage

The effect of adsorbent dosage on the removal of the MB from aqueous solution was determined using variable quantities of CRSS adsorbent ranging from 0.02 to 0.30 g at fixed volumes (100 mL) and initial dye solution where C_o was 100 mg/L. For these experiments, other operation parameters were held constant at 303 K, shaking speed of 110 stroke/min, contact time of 1,440 min, and an unadjusted pH at 5.60 for the initial MB solution. The results are shown in Fig. 5. The highest level of MB removal was achieved using 0.08 g CRSS and further addition has not significantly affected the MB removal percentage. The observed increase in the dye removal (%) with adsorbent dosage was attributed to an increase in the available adsorbent surface area, as the number of adsorption sites increase correspondingly. However, no significant changes in MB removal efficiency were observed beyond 0.08 g/100 mL CRSS dose. Due to conglomeration of adsorbent particles, there is no increase in effective surface area of CRSS. Therefore, 0.08 g of CRSS was selected for subsequent work.

3.2.2. Effect of pH

The pH of the solution influences the speciation of the dyes, along with the surface charge of the adsorbent. Fig. 6 shows the effect of variable pH from 3 to 11 on the adsorption capacity with MB. The removal of MB increased remarkably as the pH of the solution increased from 3 up to 8. Moreover, no obvious change in MB removal was seen by increasing in the pH values to higher levels (pH 8–11). The lower

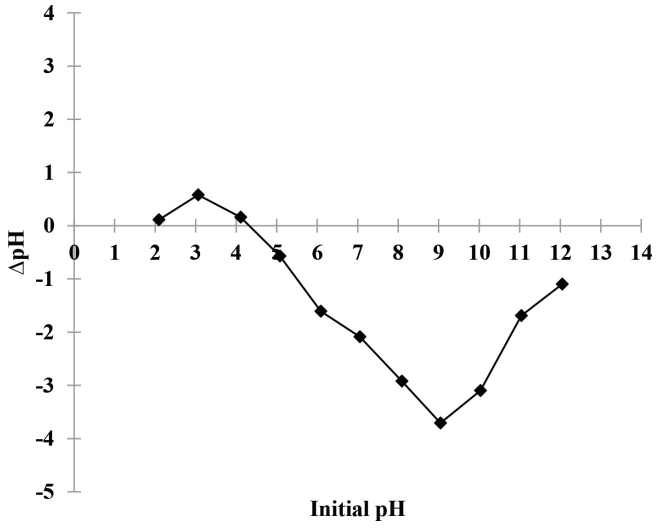

Fig. 4. pH_{pzc} of CRSS suspensions.

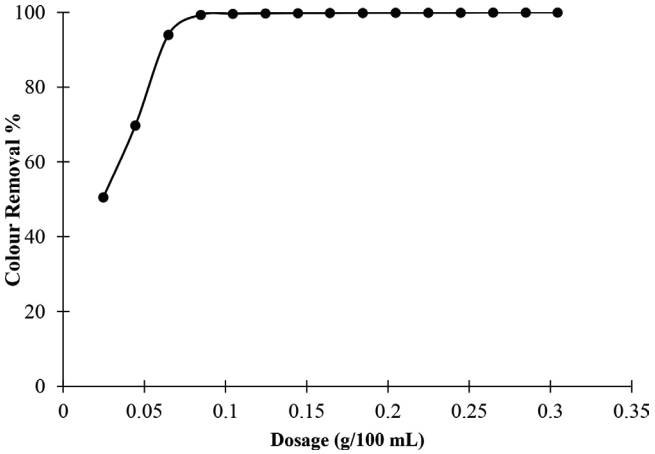

Fig. 5. Effect of CRSS dosage on MB removal (%) at $[MB]_0$ = 100 mg/L, V = 100 mL, pH = 5.6., T = 303 K, shaking speed = 110 stroke/min, and contact time = 1,440 min.

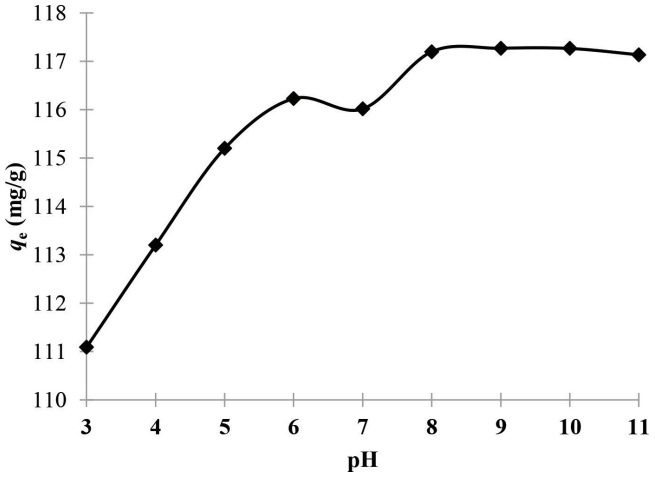

Fig. 6. Effect of pH on the adsorption capacity of MB by CRSS at $[MB]_0$ = 100 mg/L, V = 100 mL, T = 303 K, shaking speed = 110 stroke/min, contact time = 1,440 min, and CRSS dosage = 0.08 g.

adsorption of MB at acidic pH was accounted for by the competition at adsorption sites between the MB cations and excess H^+ ions in solution. At higher pH values, the surface of CRSS adopts a negative surface charge, which contributes to enhanced uptake of positively charged dye species via attractive electrostatic attraction, in accordance with an increase in the rate of adsorption [42]. Moreover, the surface of the adsorbent was positively charged, since the pH was below the PZC, where pH_{pzc} = 4.20, contributing to electrostatic repulsion of MB cations at the CRSS surface. This observation supports the results obtained from previous study of the pH_{pzc} reported by Royer et al. [33] for the removal of MB from aqueous solution using H_2SO_4-treated pine fruit shell adsorbent material. To continue this work, the effective pH for CRSS was fixed at 8, and used in further adsorption studies herein.

3.2.3. Effect of initial dye concentration and contact time

The experimental results for the adsorption properties of MB onto CRSS at various initial concentrations are shown in Fig. 7. The amount of MB adsorbed by the CRSS adsorbent at equilibrium increased rapidly from 61.5 to 236.9 mg/g as the initial dye concentration increased from 50 to 300 mg/L. Indeed, the resistance to mass transfer between the solid and aqueous phase is more easily overcome due the driving forces. The effect can be attributed to the greater rate of collision rate between MB and CRSS surface at higher initial dye concentration. Hence, additional amounts of MB were transferred to the CRSS surface. Additional time was needed to reach equilibrium for higher dye concentration because there was a tendency for MB to penetrate deeper within the interior surface of the CRSS and be adsorbed at active pore sites. This indicates that the initial dye concentration plays a significant role in the adsorption capacity of MB onto CRSS sorbent.

3.3. Adsorption isotherm

The adsorption isotherm results for CRSS were fitted using three types of isotherm models, which are Langmuir, Freundlich, and Temkin to evaluate the suitable model for describing the adsorption process. Adsorption isotherm reveals the relationship between the mass of adsorbate adsorbed per unit weight of adsorbent at equilibrium and liquid-phase equilibrium concentration of the adsorbate [37]. The Langmuir model assumes that the adsorptions occur at specific homogeneous sites on the adsorbent. As well, monolayer adsorption occurs onto a surface containing a finite number of adsorption sites with uniform adsorption and no transmigration of adsorbate on an idealized planar surface. The data of the equilibrium studies for the adsorption of MB dye onto CRSS may follow the Langmuir model [43] as in Eq. (3):

$$\frac{C_e}{q_e} = \frac{1}{q_{\max} k_L} + \frac{1}{q_{\max}} C_e \tag{3}$$

where C_e is the equilibrium concentration (mg/L) and q_e is the amount of adsorbed species per specified amount of adsorbent (mg/g), k_L is the Langmuir equilibrium constant and $q_{\max}$ is the amount of adsorbate required to form an adsorbed monolayer. Hence, a plot of C_e/q_e vs. C_e should be a straight line with a slope ($1/q_{\max}$) and an intercept ($1/q_{\max}.k_L$) as shown in Fig. 8(a). On the other hand, the Freundlich model [44] assumes heterogeneous surface energies, as described by a form of the Langmuir equation that varies as a function of the surface coverage. This model is presented as Eq. (4):

$$\ln q_e = \ln k_F + \frac{1}{n} \ln C_e \tag{4}$$

where C_e is the equilibrium concentration of the adsorbate (mg/L), q_e is the amount of adsorbate adsorbed per unit mass of adsorbent (mg/g). The affinity constant k_F (mg/g $(L/mg)^{1/n}$) relates to the adsorption capacity of the adsorbent and n is the constant which indicates the relative favorability of the adsorption process. Thus, a plot of ln q_e vs. ln C_e should be a straight line with a slope $1/n$ and an intercept of ln k_F (Fig. 8(b)). Temkin and Pyzhev [45] model considered the effects of indirect adsorbate/adsorbate interactions on adsorption isotherms. The Temkin isotherm expressed in its linear form is presented as Eq. (5) as follows:

$$q_e = B \ln k_T + B \ln C_e \tag{5}$$

where $B = (RT/b)$, a plot of q_e vs. ln C_e yielded a linear line, enables to determine the isotherm constants k_T and B (Fig. 8(c)). k_T is the Temkin equilibrium binding constant (L/mg) that corresponds to the maximum binding energy, and constant B is related to adsorption heat. The adsorption heat of all the molecules in the layer is expected to decrease linearly with coverage because of adsorbate/adsorbate interactions. The isotherms related parameters were calculated, and the results are shown in Table 2. Based on data recorded in Table 2, Langmuir model fits the data better than the Freundlich and Temkin models. This result is confirmed by the high R^2 value for the Langmuir model (0.9975) compared with the Temkin (0.9282) and Freundlich (0.7009) models. Langmuir isotherm indicates the surface homogeneity of the adsorbent. The adsorbent surface is made up of small adsorption patches, which are

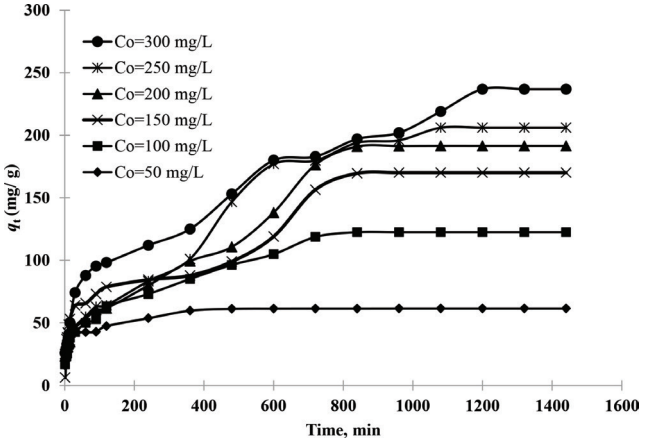

Fig. 7. Effect of initial concentration and contact time on the adsorption of MB by CRSS (V = 100 mL, T = 303 K, pH = 8, shaking speed = 110 stroke/min, and CRSS dosage = 0.08 g).

energetically equivalent to each other in terms of adsorption phenomenon [23,24]. The monolayer adsorption capacity (q_{max}) for CRSS with MB was compared with other types of H_2SO_4-treated lignocellulosic materials as recorded in Table 3. CRSS shows a relatively high adsorption capacity for MB, where q_m was 208.3 mg/g, exceeding values reported for other biomass treated with H_2SO_4 activation for the uptake of MB.

3.4. Adsorption kinetics and mechanism

The pseudo-first-order model (PFO) and pseudo-second-order model (PSO) were used to investigate the adsorption kinetics of MB dye on CRSS surface. The PFO was originally proposed by Lagergren [46] and its linearized form is given by Eq. (6) as follows:

$$\ln(q_e - q_t) = \ln q_e - k_1 t \tag{6}$$

where q_e is the amount of solute adsorbed at equilibrium per unit weight of adsorbent (mg/g), q_t is the amount of solute adsorbed at any time (mg/g), and k_1 is the adsorption constant. This expression is the most popular form of PFO model. k_1 values at different initial MB concentrations were calculated from the plots of ln ($q_e - q_t$) vs. t (Fig. 9(a)) and the values are given in Table 4. The linear form of the PSO model is given by Eq. (7) [47] as follows:

$$\frac{t}{q_t} = \frac{1}{k_2 q_e^2} + \frac{t}{q_e} \tag{7}$$

where the PSO rate constant (k_2, g/mg min) and $q_{e,cal}$ were calculated from the intercept and slope of t/q_t vs. t shown in Fig. 9(b). In Table 4, the observed R^2 values are nearly unity ($R^2 \geq 0.99$) for the PSO kinetic model, where the values of $q_{e,cal}$ are in good agreement with $q_{e,exp}$. POS kinetic model suggests that the adsorption systems studied possess chemisorption in which the attraction forces between MB molecules and the CRSS surface are due to chemical bonding. Chemisorption occurs only as a monolayer and substances chemisorbed on solid surface are hardly removed because of stronger forces at stake [48,49].

The diffusion mechanism was convinced by the intraparticle diffusion model. Experimental data were involved with Weber and Morris [50] to determine the rate of intraparticle diffusion by Eq. (8) as follows:

$$q_t = k_p t^{1/2} + C \tag{8}$$

where q_t is the adsorption capacity at time t (mg g^{-1}), k_p is the intraparticle diffusion rate constant, (mg g^{-1} min$^{-1/2}$), t is the time (min), and C is the intercept.

The graph plotted between MB uptake (q_t) and the square root of time ($t^{1/2}$) gives linear, which is considered as rate determining step [49], as shown in Fig. 10 and the values are summarized in Table 5. This is also called gradual adsorption stages which include [52–54]:

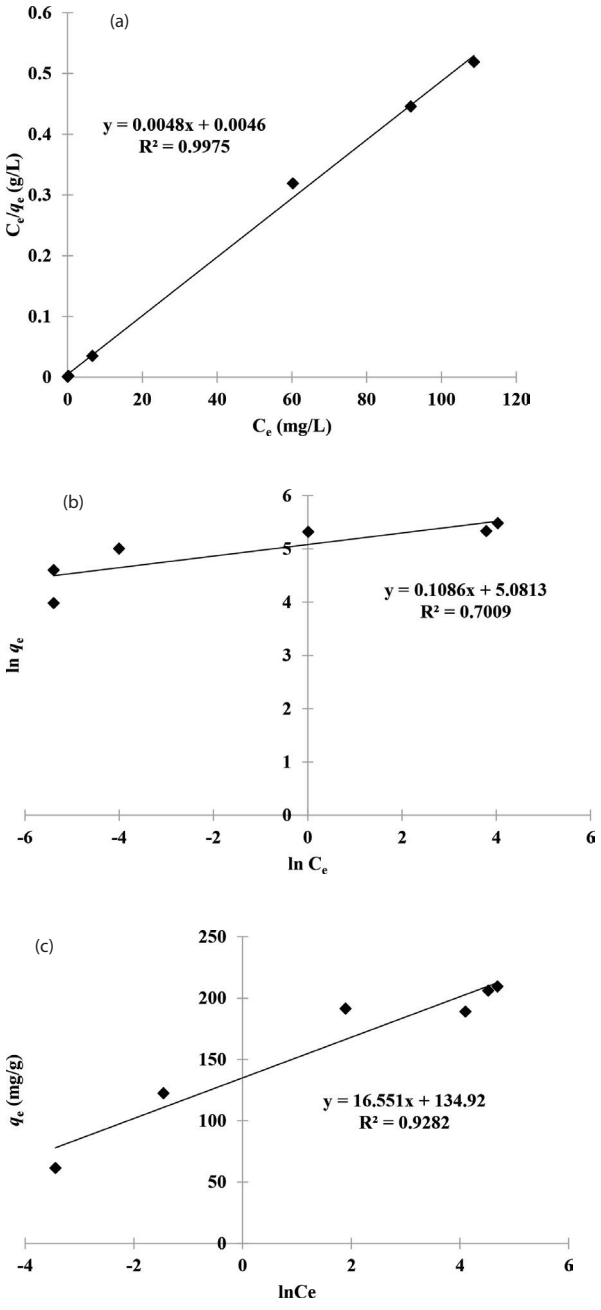

Fig. 8. Isotherm models for the adsorption of MB onto CRSS: (a) Langmuir, (b) Freundlich, and (c) Temkin.

Table 2
Isotherm parameters for adsorption of MB by CRSS at 303 K

Isotherm	Parameter	Value
Langmuir	q_m (mg/g)	208.3
	k_L (L/mg)	1.04
	R^2	0.9975
Freundlich	K_F [(mg/g) (L/mg)$^{1/n}$]	160.9
	n	0.11
	R^2	0.7009
Temkin	B	16.55
	k_T (L/mg)	2.09
	R^2	0.9282

Table 3
Comparison of adsorption capacities for MB onto different activated carbons prepared by H_2SO_4 activation

H_2SO_4-treated biomass	Adsorbent dosage, g	pH	Temperature (K)	q_{max} (mg/g)	References
Carbonized rubber seed shell (CRSS)	0.08 g/100 mL	8	303	208.3	This study
Pine-fruit shell	0.3 g/100 mL	8.5	298	529	[33]
Mango peels	0.14 g/100 mL	5–6	303	277.8	[21]
Coconut leaves	0.15 g/100 mL	6	303–323	126.9–149.3	[17]
Euphorbia rigida	0.2 g/100 mL	6	293–313	114	[28]
Bagasse	0.4 g/100 mL	9	300–333	49.8–56.5	[29]
Ficus carica	0.5 g/100 mL	8	298–323	47.6	[36]
Parthenium hysterophorus	0.4 g/100 mL	7	298	39.7	[31]
Delonix regia pods	0.2 g/100 mL	7	298	23.3	[34]
Wild carrot	0.05 g/100 mL	6	298	21	[35]
Sunflower oil cake	0.2 g/100 mL	6	288–318	16.4	[32]

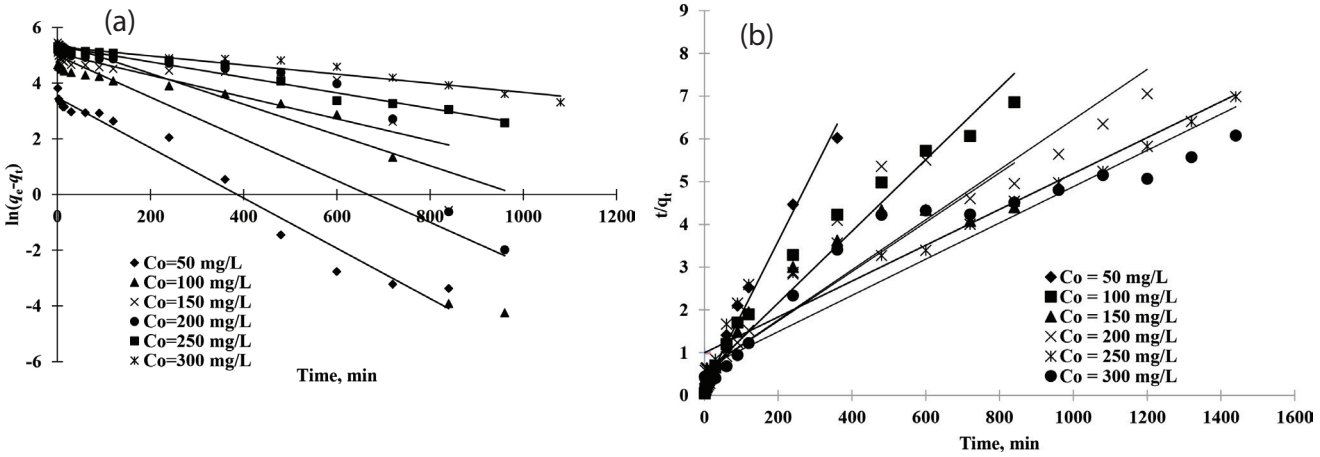

Fig. 9. Kinetic profiles for the adsorption of MB onto CRSS (a) PFO and (b) PSO.

Table 4
PFO and PSO kinetic parameters and their corresponding values at different initial dye concentrations by CRSS

Parameters	Concentration, C_o (mg/L)					
	50	100	150	200	250	300
$q_{e,exp}$ (mg/g)	61.5	122.5	170.9	191.5	206.1	236.9
PFO						
$q_{e,cal}$ (mg/g)	32.4	146.5	158.7	233.4	204.3	216.9
$k_1 \times 10^{-3}$ (1/min)	9.0	7.5	5.5	3.9	2.8	1.6
R^2	0.967	0.791	0.9770	0.660	0.981	0.938
PSO						
$q_{e,cal}$ (mg/g)	58.5	119.1	169.5	188.5	208.1	238.1
$k_2 \times 10^{-3}$ (g/mg min)	1.5	0.145	0.0576	0.0588	0.024	0.017
R^2	0.989	0.966	0.970	0.908	0.939	0.914

- the transfer of dye molecule from bulk solution to the exterior surface of the adsorbent (film diffusion)
- the transfer of dye molecule from the exterior surface to the interior surface of the pore of the adsorbent (pore diffusion)
- the dye molecules get attached to the pore wall surface of the adsorbent, active sites (adsorption).

But when these linear lines do not pass through the origin (Fig. 10), as an evident, the adsorption or sort of boundary

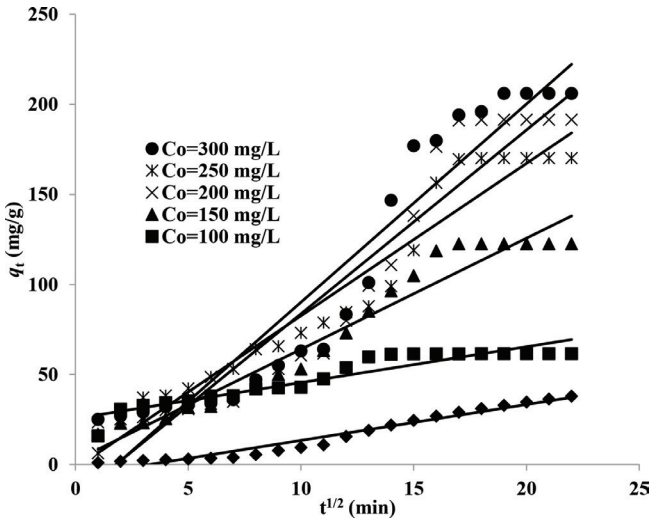

Fig. 10. Intraparticle diffusion plot for MB adsorption on CRSS at different initial concentrations (CRSS dose = 0.12 g, V = 100 ml, pH = 8, and T = 303 K).

Table 5
Intraparticle diffusion model results for the removal of MB dye by CRSS

$[MB]_0$ (mg/L)	Intraparticle diffusion model		
	k_p (mg/(g min$^{(1/2)}$))	R^2	C
50	1.99	0.95	6.48
100	6.17	0.95	18.39
150	8.46	0.94	19.93
200	10.21	0.91	22.60
250	11.01	0.91	23.38
300	11.66	0.97	25.55

layer is controlled. At this step, the rate of adsorption is limited or combined with other steps or both. Once again from the graph (Fig. 10), the linear lines do not pass through the origin, showing large number of dye molecules diffused into the pore before being adsorbed. Hence, intraparticle diffusion is not the only rate-controlling step.

4. Conclusion

From the results of the current work, it can be concluded that liquid-phase H_2SO_4 treatment of RSS agricultural waste promotes the formation of CRSS to act as a low-cost and renewable adsorbent for the removal of MB dye from aqueous solutions. Formation of acidic groups on the CRSS surface is responsible for enhancing the electrostatic and dispersion interactions between the MB and the surface functional groups of CRSS. The adsorption experiments indicated that the pseudo-second-order model provided the best description of the kinetic uptake properties, while adsorption results at equilibrium are described by the Langmuir model where the maximum adsorption capacity (q_{max}) is 208.3 mg/g.

References

[1] N.S.A. Mubarak, A.H. Jawad, W.I. Nawawi, Equilibrium, kinetic and thermodynamic studies of Reactive Red 120 dye adsorption by chitosan beads from aqueous solution, Energy Ecol. Environ., 2 (2017) 85–93.
[2] A.H. Jawad, M.A.M. Ishak, A.M. Farhan, K. Ismail, Response surface methodology approach for optimization of color removal and COD reduction of methylene blue using microwave-induced NaOH activated carbon from biomass waste, Desal. Wat. Treat., 62 (2017) 208–220.
[3] A.H. Jawad, N.S.A. Mubarak, W.I. Nawawi, Optimization of Sorption Parameters for Color Removal of Textile Dye by Cross-linked Chitosan Beads Using Box-Behnken Design, MATEC Web of Conferences, Vol. 47, 2016, p. 05009.
[4] R. Juang, S. Swei, Effect of dye nature on its adsorption from aqueous solution onto activated carbon, Sep. Sci. Technol., 31 (1996) 2143–2158.
[5] A.H. Jawad, R.A. Rashid, R.M.A. Mahmuod, M.A.M. Ishak, N.N. Kasim, K. Ismail, Adsorption of methylene blue onto coconut (*Cocos nucifera*) leaf: optimization, isotherm and kinetic studies, Desal. Wat. Treat., 57 (2016) 8839–8853.
[6] A.H. Jawad, S. Sabar, M.A.M. Ishak, L.D. Wilson, S.S.A. Norrahma, M.K. Talari, A.M. Farhan, Microwave-assisted preparation of mesoporous activated carbon from coconut (*Cocos nucifera*) leaf by H_3PO_4-activation for Methylene Blue adsorption, Chem. Eng. Commun., 204 (2017) 1143–1156.
[7] A.H. Jawad, R.A. Rashid, K. Ismail, S. Sabar, High surface area mesoporous activated carbon developed from coconut leaf by chemical activation with H_3PO_4 for adsorption of methylene blue, Desal. Wat. Treat., 74 (2017) 326–335.
[8] A.R. Khataee, A. Movafeghi, S. Torbati, S.Y. SalehiLisar, M. Zarei, Phytoremediation potential of duckweed (*Lemna minor* L.) in degradation of C.I. Acid Blue 92: artificial neural network modeling, Ecotoxicol. Environ. Saf., 80 (2012) 291–298.
[9] L. Fan, Y. Zhou, W. Yang, G. Chen, F. Yang, Electrochemical degradation of aqueous solution of Amaranth azo dye on ACF under potentiostatic model, Dyes Pigm., 76 (2008) 440–446.
[10] J.S. Wu, C.H. Liu, K.H. Chu, S.Y. Suen, Removal of cationic dye methyl violet 2B from water by cation exchange membranes, J. Membr. Sci., 309 (2008) 239–245.
[11] Y.S. Woo, M. Rafatullah, A.F.M. Al-Karkhi, T.T. Tow, Removal of Terasil Red R dye by using Fenton oxidation: a statistical analysis, Desal. Wat. Treat., 53 (2013) 1–9.
[12] A.H. Jawad, A.F.M. Alkarkhi, N.S.A. Mubarak, Photocatalytic decolorization of methylene blue by an immobilized TiO_2 film under visible light irradiation: optimization using response surface methodology (RSM), Desal. Wat. Treat., 56 (2015) 161–172.
[13] A.H. Jawad, N.S.A. Mubarak, M.A.M. Ishak, K. Ismail, W.I. Nawawi, Kinetics of photocatalytic decolourization of cationic dye using porous TiO_2 film, J. Taibah Univ. Sci., 10 (2016) 352–362.
[14] F. Akbal, Adsorption of basic dyes from aqueous solution onto pumice powder, J. Colloid Interface Sci., 286 (2005) 455–458.
[15] A.H. Jawad, M.A. Islam, B.H. Hameed, Cross-linked chitosan thin film coated onto glass plate as an effective adsorbent for adsorption of reactive orange 16, Int. J. Biol. Macromol., 95 (2017) 743–749.
[16] J. Xu, L. Chen, H. Qu, Y. Jiao, J. Xie, G. Xing, Preparation and characterization of activated carbon from reedy grass leaves by chemical activation with H_3PO_4, Appl. Surf. Sci., 320 (2014) 674–680.
[17] A.H. Jawad, R.A. Rashid, M.A.M. Ishak, L.D. Wilson, Adsorption of methylene blue onto activated carbon developed from biomass waste by H_2SO_4 activation: kinetic, equilibrium and thermodynamic studies, Desal. Wat. Treat., 57 (2016) 25194–25206.
[18] F. Marrakchi, M.J. Ahmed, W.A. Khanday, M. Asif, B.H. Hameed, Mesoporous-activated carbon prepared from chitosan flakes via single-step sodium hydroxide activation for the adsorption of methylene blue, Int. J. Biol. Macromol., 98 (2017) 233–239.

[19] L. Gao, F. Dong, Q. Dai, G. Zhong, U. Halik, D. Lee. Coal tar residues based activated carbon: preparation and characterization, J. Taiwan Inst. Chem. Eng. 63 (2016) 166–169.
[20] R. Acosta, V. Fierro, A.M. Yuso, D. Nabarlatz, A. Celzard, Tetracycline adsorption onto activated carbons produced by KOH activation of tyre pyrolysis char, Chemosphere, 149 (2016) 168–176.
[21] A.H. Jawad, N.F.H. Mamat, M.F. Abdullah, K. Ismail, Adsorption of methylene blue onto acid-treated Mango peels: kinetic, equilibrium and thermodynamic, Desal. Wat. Treat., 59 (2017) 210–219.
[22] Q.S. Liu, T. Zheng, N. Li, P. Wang, G. Abulikemu, Modification of bamboo-based activated carbon using microwave radiation and its effects on the adsorption of methylene blue, Appl. Surf. Sci., 256 (2016) 3309–3315.
[23] Y. Gokce, Z. Aktas, Nitric acid modification of activated carbon produced from waste tea and adsorption of methylene blue and phenol, Appl. Surf. Sci., 313 (2014) 352–359.
[24] H. Valdes, M. Sanchez-Polo, J. Rivera-Utrilla, C.A. Zaror, Effect of ozone treatment on surface properties of activated carbon, Langmuir, 18 (2002) 2111–2116.
[25] N.A. Oladoja, Studies on the sorption of basic dye by rubber (*Hevea brasiliensis*) seed shell, Turkish J. Eng. Environ. Sci., 32 (2008) 143–152.
[26] L.O. Ekebafe, J.E. Imanah, F.E. Okieimen, Effect of carbonization on the processing characteristics of rubber seed shell, Arab. J. Chem., 10 (2017) S174–S178.
[27] B.H. Hameed, F.B.M. Daud, Adsorption studies of basic dye on activated carbon derived from agricultural waste: *Hevea brasiliensis* seed coat, Chem. Eng. J., 139 (2008) 48–55.
[28] Ö. Gerçel, A. Özcan, A.S. Özcan, H.F. Gerçel, Preparation of activated carbon from a renewable bio-plant of *Euphorbia rigida* by H_2SO_4 activation and its adsorption behavior in aqueous solutions, Appl. Surf. Sci., 253 (2007) 4843–4852.
[29] L.W. Low, T.T. Teng, A. Ahmad, N. Morad, Y.S. Wong, A novel pretreatment method of lignocellulosic material as adsorbent and kinetic study of dye waste adsorption, Water Air Soil Pollut., 218 (2011) 293–306.
[30] H. Hasar, Adsorption of nickel (II) from aqueous solution onto activated carbon prepared from almond husk, J. Hazard. Mater., 97 (2003) 49–57.
[31] H. Lata, V.K. Garg, R.K. Gupta, Removal of a basic dye from aqueous solution by adsorption using *Parthenium hysterophorus*: an agricultural waste, Dyes Pigm., 74 (2007) 653–658.
[32] S. Karagöz, T. Tay, S. Ucar, M. Erdem, Activated carbons from waste biomass by sulfuric acid activation and their use on methylene blue adsorption, Bioresour. Technol., 99 (2008) 6214–6222.
[33] B. Royer, N.F. Cardoso, E.C. Lima, J.C.P. Vaghetti, R.C. Veses, Applications of Brazilian pine-fruit shell in natural and carbonized forms as adsorbents to removal of methylene blue from aqueous solutions: kinetics and equilibrium study, J. Hazard. Mater., 164 (2009) 1213–1222.
[34] Y.S. Ho, R. Malaryvizhi, N. Sulochana, Equilibrium isotherm studies of methylene blue adsorption onto activated carbon prepared from *Delonix regia* pods, J. Environ. Prot. Sci., 3 (2009) 1–6.
[35] M. Mahadeva Swamy, B.M. Nagabhushana, R. Hari Krishna, Nagaraju Kottam, R.S. Raveendra, P.A. Prashanth, Fast adsorptive removal of methylene blue dye from aqueous solution onto a wild carrot flower activated carbon: isotherms and kinetics studies, Desal. Wat. Treat., 71 (2017) 399–405.
[36] D. Pathania, S. Sharma, P. Singh, Removal of methylene blue by adsorption onto activated carbon developed from *Ficus carica* bast, Arab. J. Chem., 10 (2017) S1445–S1451.
[37] N. Sharma, D.P. Tiwari, S.K. Singh, The efficiency appraisal for removal of malachite green by potato peel and neem bark: isotherm and kinetic studies, Int. J. Chem. Environ. Eng., 5 (2014) 83–88.
[38] V.K. Garg, R. Kumar, R. Gupta, Removal of malachite green dye from aqueous solution by adsorption using agro-industry waste: a case study of *Prosopis cineraria*, Dyes Pigm., 62 (2004) 1–10.
[39] M.V. Lopez-Ramon, F. Stoeckli, C. Moreno-Castilla, F. Carrasco-Marin, On the characterization of acidic and basic surface sites on carbons by various techniques, Carbon, 37 (1999) 1215– 1221.
[40] Z. Jiang, Y. Liu, X. Sun, F. Tian, F. Sun, C. Liang, W. You, C. Han, C. Li, Activated carbons chemically modified by concentrated H_2SO_4 for the adsorption of the pollutants from wastewater and the dibenzothiophene from fuel oils, Langmuir, 19 (2003) 731–736.
[41] R.A. Rashid, A.H. Jawad, M.A.M. Ishak, N.N. Kasim, KOH-activated carbon developed from biomass waste: adsorption equilibrium, kinetic and thermodynamic studies for Methylene blue uptake, Desal. Wat. Treat., 57 (2016) 27226–27236.
[42] S. Chakraborty, S. Chowdhury, P.D. Saha, Adsorption of Crystal Violet from aqueous solution onto NaOH modified rice husk, Carbohydr. Polym., 86 (2011) 1533–1541.
[43] I. Langmuir, The adsorption of gases on plane surfaces of glass, mica and platinum, J. Am. Chem. Soc., 40 (1918) 1361–1403.
[44] H. Freundlich, Ueber die adsorption in Loesungen (Adsorption in solution), Z. Phys. Chem., 57 (1906) 385–470.
[45] M.J. Temkin, V. Pyzhev, Recent modifications to Langmuir isotherms, Acta Physiochim. USSR, 12 (1940) 217–222.
[46] S. Lagergren, Zur theorie der sogenannten adsorption geloster stoffe, K. Sven. Vetensk.akad. Handl., 24 (1898) 1–39.
[47] Y.S. Ho, G. McKay, Sorption of dye from aqueous solution by peat, Chem. Eng. J., 70 (1998) 115–124.
[48] R.A. Rashid, M.A.M. Ishak, K.M. Hello, Adsorptive removal of methylene blue by commercial coconut shell activated carbon, Sci. Lett., 12 (2018) 27–97.
[49] A.H. Jawad, Y.S. Ngoh, K.A. Radzun, Utilization of watermelon (*Citrullus lanatus*) rinds as a natural low-cost biosorbent for adsorption of methylene blue: kinetic, equilibrium and thermodynamic studies, J. Taibah Univ. Sci., 12 (2018) 371–381.
[50] W.J. Weber, J.C. Morris, Kinetics of adsorption on carbon from solution, J. Sanit. Eng. Div. Am. Soc. Civ. Eng., 89 (1963) 31–60.
[51] S. Suganya, S. Kumar, A. Saravanan, C. Ravikumar, Computation of adsorption parameters for the removal of dye from wastewater by microwave assisted sawdust: theoretical and experimental analysis, Environ. Toxicol. Pharmacol., 50 (2017) 45–57.
[52] P. Senthil Kumar, P.S.A. Fernando, R.T. Ahmed, R, Srinath, M. Priyadharshini, A.M. Vignesh, A. Thanjiappan, Effect of temperature on the adsorption of methylene blue dye onto sulfuric acid–treated orange peel, Chem. Eng. Commun., 201 (2014) 1526–1547.
[53] P.S. Kumar, S. Ramalingam, C. Senthamarai, M. Niranjanaa, P. Vijayalakshmi, S. Sivanesan, Adsorption of dye from aqueous solution by cashew nut shell: studies on equilibrium isotherm, kinetics and thermodynamics of interactions, Desalination, 261 (2010) 52–60.
[54] P. Senthil Kumar, R. Sivaranjanee, U. Vinothini, M. Raghavi, K. Rajasekar, K. Ramakrishnan, Adsorption of dye onto raw and surface modified tamarind seeds: isotherms, process design, kinetics and mechanism, Desal. Wat. Treat., 52 (2010) 2620–2633.